Experimental Mechanics (2012) 52:1447–1459
DOI 10.1007/s11340-012-9600-x

Technique of Measuring Piston Secondary Motion Using Laser Displacement Sensors

Y.-C. Tan · Z.M. Ripin

Received: 7 September 2011 / Accepted: 30 January 2012 / Published online: 25 February 2012

Abstract An experimental technique for measuring the distinct modes of piston secondary motion is described in this study. The measurement system consists of three laser displacement sensors with the laser spots aimed at the piston crown, where the target area is machined with flat slot and a 45° slope profile to provide the necessary reflective angle in order to obtain the rotational and lateral motion of the piston head. The Pearson's correlation coefficient revealed a strong relationship between the rotational motion and the lateral motion of the piston at a low engine speed of 100 rpm, and this correlation is weakened as the speed increases up to 500 rpm. The lateral motion results captured by the laser displacement sensor are verified by comparing the frequency components of the lateral motion with the frequency components of the lateral acceleration measured using a triaxial accelerometer. The measurements of the distinct modes of the piston secondary motion are shown to be valid and reasonable.

Keywords Piston secondary motion · Piston lateral motion · Piston rotational motion · Piston lateral acceleration · Laser displacement sensors

Introduction

The piston secondary motion in an internal combustion engine is one of the major sources of engine noise. This engine noise is the piston slap noise generated by the impact of the piston skirt on the cylinder liner. Although the clearance between the piston skirt and the cylinder liner is very small, the piston secondary motion inside the cylinder liner is sufficient to generate this undesirable piston slap noise and subsequent engine block vibration [1]. The clearance between the piston and cylinder liner can be defined as a translational clearance joint. The clearance restricts the amplitude of the piston motion inside the cylinder bore and does not affect any degree of freedom of the piston slider mechanism [2]. Therefore, this clearance allows the piston to move in the lateral direction and tilt along the piston pin axis within a limited amplitude, and these motions are superimposed on the piston reciprocating motion. A number of studies have been carried out classifying the motion of the piston in the cylinder bore into four different modes [2–6]:

- Translational motion of a piston inside a cylinder bore without any contact between the piston skirt and cylinder liner.
- Lateral motion of a piston, which causes the two adjacent corners of the piston skirt to be in contact with the cylinder liner.
- Rotational motion of a piston along its piston pin axis, which causes one or more of the diagonal corners of the piston skirt to be in contact with the cylinder liner.
- A piston translating inside the cylinder liner with both lateral motion and rotational motion, and the piston skirt is in contact with the cylinder liner.

Kim [7] carried out numerical analysis of the piston secondary motion of a small refrigeration reciprocating compressor. The developed model was used to calculate the piston trajectory in order to analyze the piston secondary motion of the reciprocating piston. The study showed that radial clearance, oil viscosity, piston pin location, and piston skirt length have strong influences on the piston dynamics.

Y.-C. Tan · Z. Ripin (✉)
School of Mechanical Engineering, Universiti Sains Malaysia,
14300 Nibong Tebal, SPS,
Pulau Pinang, Malaysia
e-mail: mezaidi@eng.usm.my

Cho and Moon [8] studied the piston dynamic response by applying the finite element method (FEM) and finite difference method (FDM). The lubrication structure of the reciprocating compressor was obtained from the coupling of the lubricating pressure with the piston dynamic motion by using the FEM. The piston secondary motion was shown to be influenced by the piston axis eccentricity and tilting angle. In addition to the compression pressure, the piston secondary motion also influences the distribution of the oil film pressure, and the location of the wrist pin is important to the engine performance.

Geng and Chen [9] developed a two-degree-of-freedom nonlinear mathematical model to simulate the piston secondary motion and investigated the piston-slap–induced vibration. The vibration response of the cylinder block excited by the piston slap increases with increasing engine operating speeds and piston clearances. Another mathematical model was constructed by considering the coupling of the piston secondary motion and variation of the system inertia to analyze the piston lubrication. The results showed that the piston secondary motion was greatly affected by the variation of system inertia, engine operating speed, and center of gravity of the connecting rod [10, 11].

A coupled model of piston secondary motion and piston assembly oil film lubrication was developed by Zhou et al. [12]. The effect of the piston ring tribological behaviors and the waviness of the piston bore were considered in this dynamics model. The results showed that the piston secondary motion has a significant impact on the piston assembly lubrication, which in turn affects the piston dynamics.

A recent dynamic analysis of piston secondary motion by McFadden and Turnbull [13] based on the universal average Reynolds equation showed that the behavior of the piston secondary motion was suppressed by the lubricant film pressure under the fully flooded lubrication condition and that the lateral motion and rotational motion became more steady compared to the rapid piston secondary motion under dry conditions. The existence of a lubrication oil film in between the surfaces of the piston skirt and cylinder liner under the fully flooded lubrication condition prevented the elastic contact in dry conditions.

There has been only one experimental result reported on secondary motion measurement, an indirect measurement of the piston secondary motion of a diesel engine reported by Cho et al. [1]. In this study, accelerometers were mounted on the engine block surface to measure the engine block surface's vibration velocity level. The secondary motion of the piston was predicted using a convolution of the impact force calculated from the model.

There has been no experimental work carried out to verify directly the basic modes of piston motion listed above. Study of the piston secondary motion is important, since the likelihood of contact between the piston skirt and the cylinder liner is likely to increase as the piston secondary motion increases. The friction loss of the piston ring assembly, comprising the piston skirt and piston ring pack, is the largest component of the total engine mechanical loss and, by some estimates, makes up 45–50% of the total mechanical loss [14]. The friction loss of the piston skirt is another of the highest single components contributing to the total engine mechanical loss, after that of the piston ring [15]. Moreover, the dramatic increase in friction due to the contact between the piston skirt and the cylinder liner will cause degradation and breakdown of the lubrication oil film, which will bring about scuffing [16] and may cause seizure of the interface between the piston skirt and the cylinder liner [17].

In the authors' previous study [18], an experimental rig was developed to investigate the frictional behavior of the piston rings of a two-stroke engine under piston secondary motion. Only rotational motion of the piston secondary motion was captured by laser displacement sensors that measured the tilt angle of the piston along the piston pin axis. However, the type of motion involved was not analyzed. In this study, the experimental technique was expanded to capture the piston lateral and rotational motion distinctly by using three laser displacement sensors under non-firing conditions. This is the first time that the secondary motion of the piston has been fully captured for all the modes and that the frequency of each mode has been determined. These results are important because they will enable better understanding of the nature of the secondary motion of the piston and the influence of each mode on the piston slap.

Hardware Implementation

Construction of Measurement System

An experimental rig was designed and fabricated as shown in Fig. 1, and a 126 cc four-stroke motorcycle engine block is used in this study. The geometric and physical properties of the piston assembly are shown in Fig. 2 and Table 1. The piston assembly does not allow firing, and the crankshaft of the piston assembly was driven by an AC motor (MarelliMotori MAA80 MB4) controlled by a variable frequency controller (Emerson Commander SK).

Piston Motion Measurement

A measurement system consisting of three laser displacement sensors (Keyence LK-G152) is located at the front of the piston

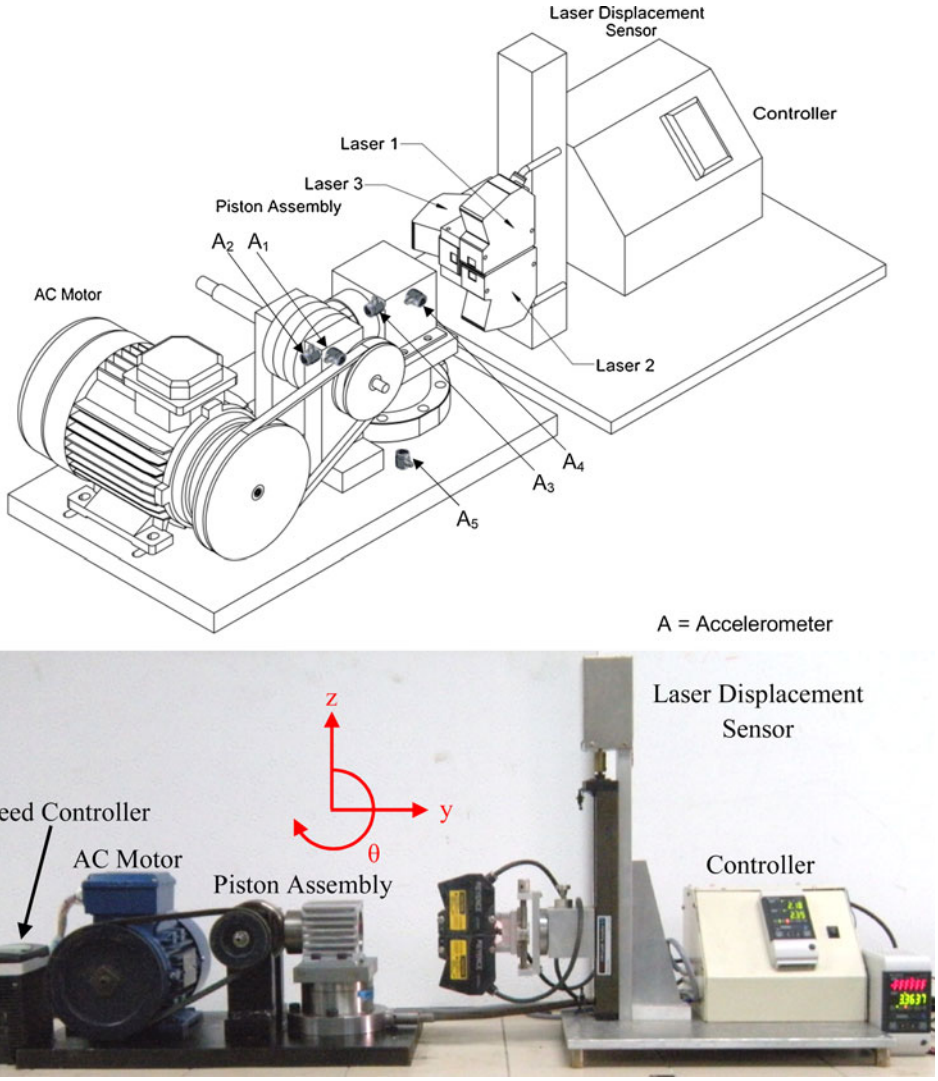

Fig. 1 Schematic and photograph of experimental setup for the piston secondary motion measurement system

assembly, and the three laser spots are aimed at three different locations on piston crown. In order to capture the different piston secondary motion, two laser spots, L_1 and L_2, are directed toward the surface of a 24-mm-long flat slot located on the right side of the piston head surface to capture the piston rotational motion, while the other laser spot, L_3, is directed toward the 45° slope profile located on the left side of the piston head surface, which has a slope height h_1 of 2 mm, to capture the piston lateral motion. The arrangement of the laser spots on the piston head is shown in Fig. 3. In order to limit the signal to the one related to the piston secondary motion, a low-pass filter with a cutoff frequency of 300 Hz is used.

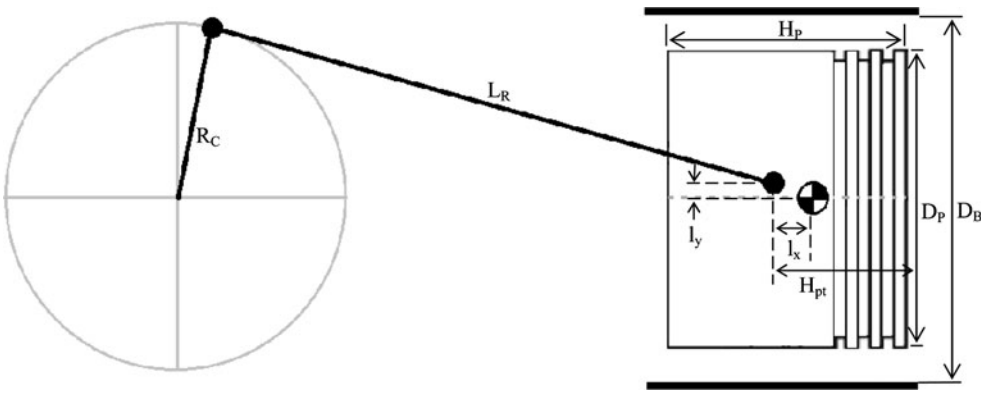

Fig. 2 Schematic diagram of the piston assembly

Table 1 Specifications of piston assembly

Description	Specification
Piston Mass (kg)	0.105
Crank Radius (mm)	28.5
Displacement (cc)	127.6
Bore Diameter, D_B (mm)	57
Stroke (mm)	50
Radial Clearance, $D_B - D_P$ (mm)	0.50
Piston Height, H_P (mm)	45
Piston pin offset from C.G., l_x (mm)	10
Piston pin offset from the bore center, l_y (mm)	0.5
Distance between cross pin center and piston top, H_{pt} (mm)	20.5

Verification of the Measurement System

A miniature triaxial accelerometer (Dytran 3023 M20) is mounted at the center of the piston crown, as shown in Fig. 3, to capture the lateral acceleration component of the piston. The *z*-axis of the accelerometer is positioned in the direction lateral to the piston travel. The frequency spectrum of the lateral acceleration signal will be used to verify the frequency component of the piston lateral motion measured by the laser displacement sensors.

FFT of Piston Motion

Fast Fourier transform (FFT) analysis is used here to identify the different modes of the piston motion. The time series data of the reciprocating motion, rotational motion, and impact acceleration captured by the triaxial accelerometer are analyzed online and transformed into the frequency domain by the IMC data acquisition system [19]. The Hanning window is chosen in the FFT analyzer with 1024 FFT points. The frequency spectrum of the piston lateral motion is obtained offline after processing the data of laser displacement sensor using the formula shown in Section "Technique for Motion Classification" to obtain the different modes of the piston secondary motion.

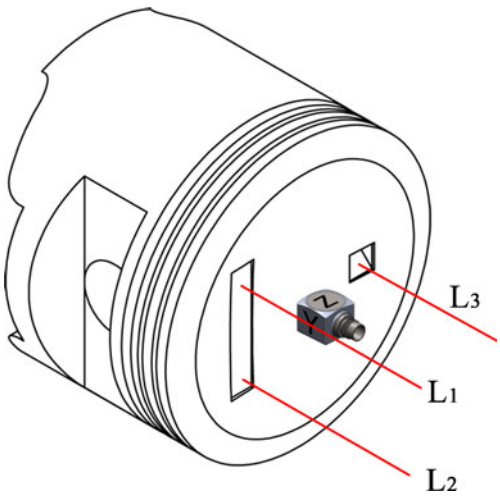

Fig. 3 Machining flat slot and 45° slope profile on piston crown and location of the mounted triaxial accelerometer

Spectral Analysis of the Experimental Rig

Spectral analysis was carried out on the experimental rig to determine the vibration level under the operating conditions in order to determine the effect of the induced vibration of the experimental rig components such as the bearing housing, pulley, V-belt, and steel base plate on the piston motion. The vibration level of the experimental rig was measured using five accelerometers (Dytran 3055B2T), with two accelerometers (A_1 and A_2) mounted on the bearing housing, two accelerometers (A_3 and A_4) on the cylinder block, and one accelerometer (A_5) mounted on the steel base plate, as shown in Fig. 1. The accelerometers mounted on the bearing housing and cylinder block measure the acceleration level in the *x* and *y* directions, and the accelerometer mounted on the steel base plate measures the acceleration level in the *z* direction. All the accelerometers are connected to the LMS Scadas Mobile data acquisition system and the LMS Test Lab post-processing software. The measurement of the experimental rig was carried out at an AC motor driving speed of 500 rpm (8.33 Hz), which is the highest operating speed of the piston motion study.

Figure 4 shows the FFT of the acceleration level of the experimental rig in the *x*, *y*, and *z* directions. The results show that the highest vibration amplitude of the bearing housing and cylinder block in the *y* direction, which is the piston reciprocating direction, was 0.53×10^{-3} m/s^2, while the acceleration level in the *x* direction is 1.7×10^{-3} m/s^2 at 0.4 Hz, and the acceleration level of the steel base plate in the *z* direction, which corresponds to the lateral motion direction, is 0.3×10^{-3} m/s^2. These results show that the effect of the vibration of the experimental rig components induced by the AC motor on the piston motion is insignificant at operating speeds below 500 rpm.

Technique for Motion Classification

The first two laser spots (L_1 and L_2) are aimed at the flat slot on the piston crown to capture the piston tilt angle, and the third laser spot (L_3) is aimed at the sloped surface to

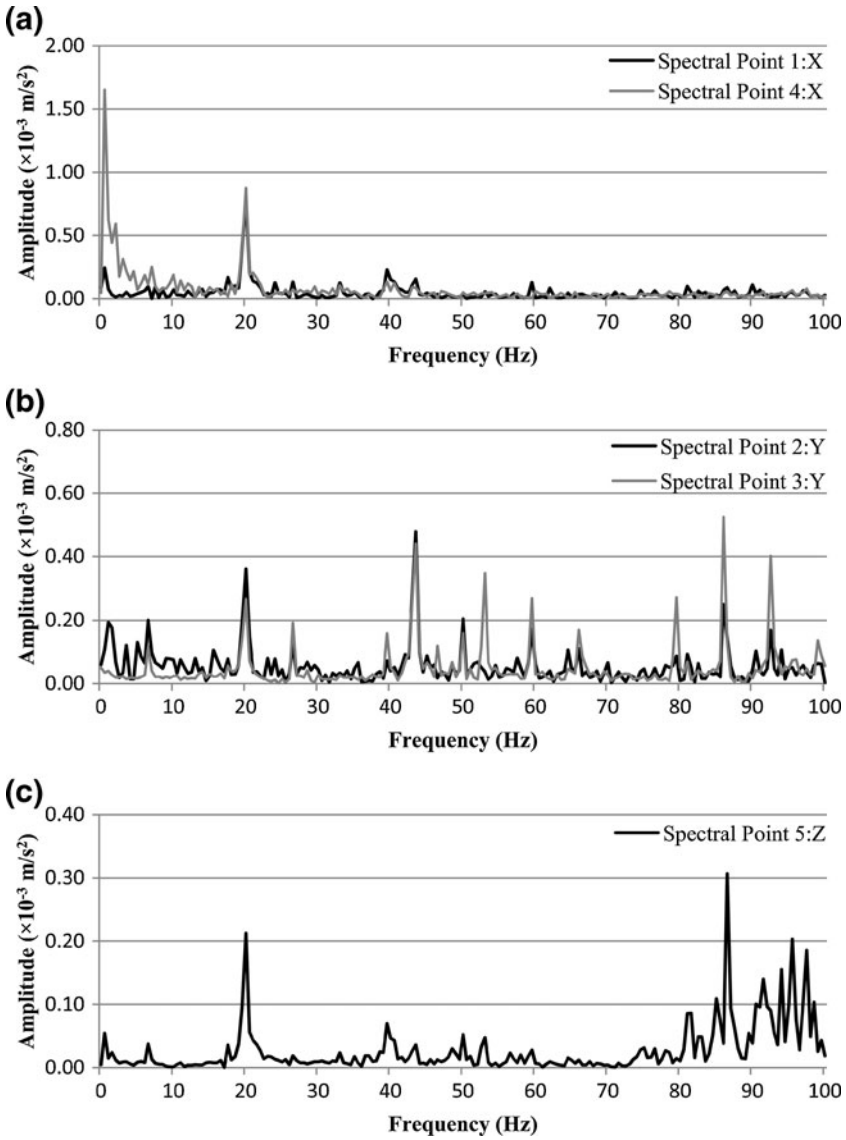

Fig. 4 Spectral analysis FFT results for (**a**) x direction, (**b**) y direction, and (**c**) z direction

determine the piston lateral motion, as shown in Fig. 3. The piston secondary motion can be further classified into four different components, which are pure translational motion, pure lateral motion, pure rotational motion, and a combination of lateral motion and rotational motion, as shown in Fig. 5.

For the first mode, which represents pure translational motion of the piston inside the cylinder bore, as shown in Fig. 5(a), the difference between L_1 and L_2 is 0, as there is no relative horizontal displacement between the two laser spots. This condition is represented by the equation below:

$$L_1 - L_2 = 0 \tag{1}$$

In order to confirm that the motion is purely translational, an additional condition is set that requires the difference between L_3 and the piston crown center displacement x_c to be equal to 0, as shown in equation (2), because during purely translation motion the laser spot of L_3 remains stationary on the slope surface, and thus there is no relative horizontal displacement between these two points.

$$\Delta L_3 = L_3 - x_c = dx = 0 \tag{2}$$

The value of x_c can be obtained as the mean value of L_1 and L_2, as shown below:

$$x_c = \frac{L_1 + L_2}{2} \tag{3}$$

For the second mode, when the piston undergoes lateral motion perpendicular to the cylinder axis, the two adjacent corners of the piston skirt will come into contact with the cylinder liner, as shown in Fig. 5(b). The difference between L_1 and L_2 in equation (1)

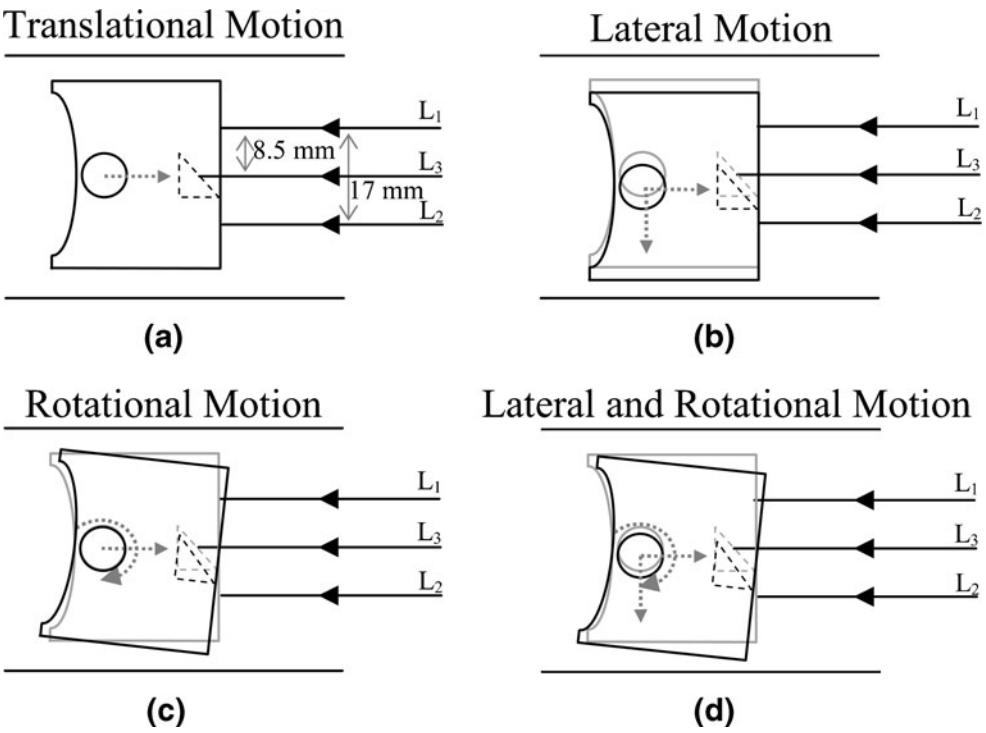

Fig. 5 Modes of piston motions

remains 0, as there is no relative horizontal displacement between the two laser spots. However, L_3 slides along the slope surface, resulting in a relative horizontal displacement between L_3 and the center of the piston crown, called dx, as shown below:

$$\Delta L_3 = L_3 - x_c = dx \neq 0 \tag{4}$$

Therefore, the vertical displacement of lateral motion of the piston can be obtained from ΔL_3 which is the horizontal component of the slope surface with the slope angle $\phi = 45°$:

$$dy = dx \cdot \tan 45 \tag{5}$$

For the third mode, which is pure rotational motion of the piston about the pin axis, as shown in Fig. 5(c), the angular displacement, θ_1, can be determined from the relative displacement of L_1 and L_2 as

$$L_1 - L_2 \neq 0 \tag{6}$$

$$\theta_1 = \tan^{-1}\left(\frac{L_1 - L_2}{17}\right) \tag{7}$$

In order to confirm that the motion is pure rotational motion, the value of the tilt angle of the piston can be calculated by using ΔL_3 data, since the laser spot slides along the slope surface during the piston rotation, which results in a change in the relative displacement between L_3 and the piston crown center, x_c. This tilt angle is denoted as θ_2 in the following equations:

$$\Delta {L_3}^1 = L_3 - x_c = \frac{h_1}{2}\left\{\frac{1}{\tan\phi} - \frac{1}{\tan(\phi + \theta_2)}\right\} \tag{8}$$

$$\theta_2 = \tan^{-1}\left\{\left(\frac{1}{\tan\phi} - \frac{2 \cdot \Delta L_3}{h}\right)^{-1}\right\} - \phi \tag{9}$$

The condition for pure rotational motion is met when both tilt angles θ_1 and θ_2 obtained from equations (7) and (9) have the same value:

$$\theta_1 = \theta_2 \tag{10}$$

The tilt angle θ_1 from equation (7) can be substituted into equation (8), as

$$\Delta {L_3}^2 = \frac{h_1}{2}\left\{\frac{1}{\tan\phi} - \frac{1}{\tan(\phi + \theta_1)}\right\} \tag{11}$$

The resulting change in ΔL_3 is 0, as shown below:

$$\Delta {L_3}^1 - \Delta {L_3}^2 = 0 = dx \tag{12}$$

Therefore, the change in the value of ΔL_3 in the lateral direction is 0,

$$dx = 0; dy = 0 \tag{13}$$

For the fourth mode of combined lateral and rotational motion, as shown in Fig. 5(d), the tilt angles obtained from equations (7) and (9) will not be equal,

$$\theta_1 - \theta_2 \neq 0 \tag{14}$$

Therefore, the tilt angle θ_1 obtained from equation (7) is substituted into equation (8) to acquire the actual change in L_3 caused by the rotational motion. The difference between equations (8) and (11) obtained in equation (15) represents the lateral movement of the piston, as shown below:

$$\Delta {L_3}^1 - \Delta {L_3}^2 = dx \neq 0 \tag{15}$$

$$\because dy = dx \cdot \tan 45 \tag{16}$$

The equations above provide the conditions for the four different modes of the secondary motion of the piston.

Results and Discussion

Piston Secondary Motion

The piston motion was captured by using three laser displacement sensors, and the three components of the motion, which include reciprocating, rotational, and lateral motion of the piston head, were calculated offline based on the equations in Section "Technique for Motion Classification". The piston motion is shown for various speeds (100, 200, 300, and 500 rpm) in Fig. 6. In the graphs in Fig. 6, the *Y*-axis on the left side represents the reciprocating motion of the piston head, while the *Y*-axis on the right side represents the tilt angle of the piston head during the rotational motion and piston lateral motion in the vertical direction. The range of lateral motion and of the tilt angle of the piston head at a speed of 100 rpm are 0–0.45 mm and −0.1–0.5°, respectively. As the engine speed increases to 200 rpm, the range of the lateral motion and of tilt angle of the piston head become 0–0.46 mm and −0.1–0.5°, respectively. At 300 rpm, the range of lateral motion is 0–0.45 mm, and the maximum tilt angle is 0.52°. The maximum displacement of the lateral motion increases to 0.5 mm and maximum tilt angle reaches 0.58° as the engine speed increases to 500 rpm. The values for the maximum lateral motion and the tilt angle are still below the piston clearance of 0.5 mm and the angular clearance of 0.64°, which indicates that the results obtained are reasonable and within bounds. Figure 7 shows the maximum tilt angle of the piston throughout the cycle. Because of the gap and the clearance, nonlinear motion exists, which resulted in an unsmooth secondary motion, unlike the sinusoidal wave of the primary motion. The tilt angle measurement is performed throughout the cycle. The value of the maximum tilt angle is obtained from Fig. 6, and it generally occurred in or around the top dead center (TDC) position. These maximum angles are then used as a set of data, as shown in Fig. 7. The increase in the maximum tilt angle with increasing speed indicates the effect of the increase in the inertia due to the combination of the rotational motion and linear motion of the connecting rod. Since the inertia force due to the rotational motion of the connecting rod is a function of ω^2, it is expected that this force, when acting on the piston pin (which is offset by 10 mm from the center of gravity of the piston), will cause a moment about the center of gravity, resulting in an increase of the tilt angle. This effect has also been observed in the numerical analyses performed by Cho et al. [1], Geng and Chen [9], and Farahanchi and Shaw [20]. However, the value of the maximum tilt angle is bounded by the clearance between the piston and the cylinder. From Fig. 6 it can be observed that as the engine speed increases, the phase angle between the motions increases. Figure 6(a) shows a phase angle between the three motions at 100 rpm of 4.5°. However, as the engine speed increases to 500 rpm, the phase angle increases to 20.3°. This is more apparent in the development of the phase angle between the rotational motion and the lateral motion, as shown in Fig. 6(d). In general, the rotational motion and the lateral motion did not produce smooth lines because of the nonlinear effect of the clearance between the piston and the cylinder liner. The phase angle is determined based on the positions of the peak and trough of each curve, and the distances between individual peaks and troughs are measured. The increase in the phase angle between the rotational motion and lateral motion with increasing speed is a new result in the study of the secondary motion of the piston. Future models of the piston secondary motion will need to include this effect. Another important observation is that the duration of piston sliding increases with increasing speeds. At a low speed of 100 rpm, the duration of the piston sliding motion is $T/8$ ($0.125T$), where T is the period of crankshaft rotation, and at a speed of 500 rpm, the piston sliding lasted for $13T/48$ ($0.27T$). All these observations are important in the analysis of piston secondary motion, as they have not been reported previously in either experimental work [1] or numerical modeling [8, 20–22]. The rotational motion of the piston head increases gradually as the piston head travels from bottom dead center (BDC) to TDC. The maximum tilt angle of the piston head occurs at TDC and declines slowly to a minimum at BDC. The changes in the lateral motion of the piston head show a similar trend to the change in the rotational

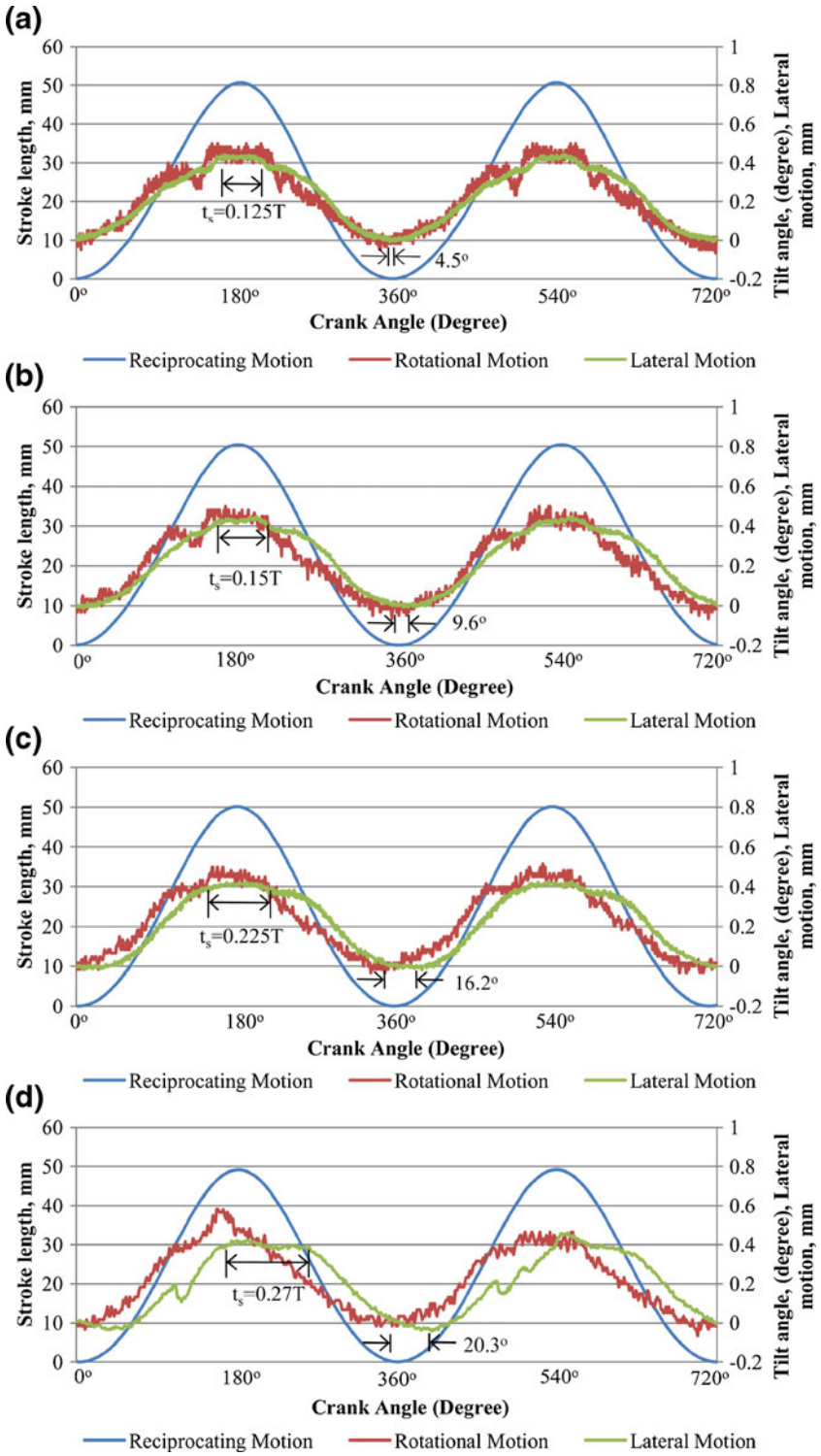

Fig. 6 Piston rotational motion and lateral motion at (**a**) 100 rpm, (**b**) 200 rpm, (**c**) 300 rpm, and (d) 500 rpm

motion of the piston head. Table 2 shows the Pearson's correlation coefficient of the piston tilt angle and lateral motion at various speeds. At a low speed of 100 rpm, the piston lateral motion shows a very strong association with the piston rotational motion, with a Pearson's correlation coefficient of 0.96. As the engine speed increases to 200 rpm and 300 rpm, the Pearson's correlation coefficient declines to 0.93 and 0.90. The *r* value drops to 0.7 as the engine speed further increases to 500 rpm, showing that the dependence between the piston lateral motion and piston tilt angle weakens with increasing speeds. Obviously, this phenomenon reveals that the interdependence of the tilt angle and the lateral motion of the piston

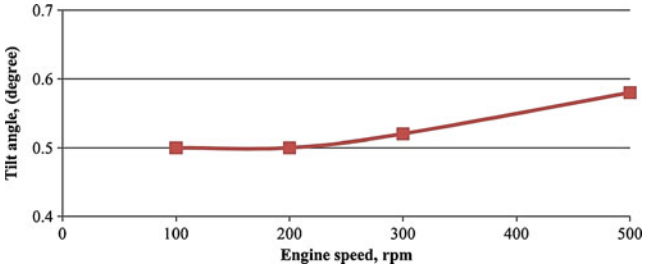

Fig. 7 Maximum tilt angle of rotational motion at different engine speeds

head are speed dependent, and are influenced by the engine operating speed.

The clearance between the piston skirt and the cylinder bore produces a nonlinear effect on the motion of the piston. The existence of the clearance does not constrain any degree of freedom of the piston, but it imposes some restrictions on the piston motion inside the cylinder bore, which limits the lateral displacement and the tilt angle of the piston. However, the nonlinear effect is due to the impact (piston slap) and temporary loss of contact between the piston and the cylinder. These two factors have been included in the model of a translational joint with clearance by Flores et al. [2, 22].

Verification of the Measurement System

A triaxial miniature accelerometer (Dytran 3023 M20) is mounted on the surface of the piston crown with the *z*-axis of the accelerometer lying in the transverse direction to the direction of piston reciprocation so as to capture the lateral acceleration. Figures 8, 9 and 10 show the frequency spectra of lateral motion and lateral acceleration obtained by FFT analysis at 100 rpm, 200 rpm, and 300 rpm, respectively. The highest amplitude of the lateral acceleration occurred at the first harmonic mode of 100 rpm, 200 rpm, and 300 rpm, with amplitudes of 0.72 ms^{-2} at 1.51 Hz, 1.46 ms^{-2} at 3.22 Hz, and 2.44 ms^{-2} at 4.98 Hz, respectively. The measurement of the acceleration in the lateral direction is used to verify the frequency component of the lateral displacement measured by the laser displacement sensor. The frequency components of the first six modes of the lateral acceleration captured by the accelerometer showed similar frequencies to those of the lateral motion measured using laser displacements sensors. Thus, the technique of measuring piston lateral motion by laser displacement sensors are proven to be valid.

Table 2 Pearson's correlation of rotational motion and lateral motion

Speed (rpm)	Pearson's correlation coefficient, *r*
100	0.96
200	0.93
300	0.89
500	0.70

Mode of Piston Motion

Figures 11 and 12 show the frequency spectrum of the piston lateral motion at 500 rpm and rotational motion obtained using FFT analysis at 100 rpm, 200 rpm, 300 rpm, and 500 rpm. From Fig. 12(a), the frequency spectrum of the piston rotational motion consists of eight harmonic modes with amplitudes of the tilt angle from 0.01° to 0.18°. The dominant frequency is still 1×, and the 2×, 3×, and 5× frequencies all have less strength. All other harmonics remain weak. There are four harmonic modes in the frequency spectrum of the piston lateral motion with amplitudes of the lateral displacement from 0.01 mm to 0.22 mm, as shown in Fig. 8(a). Again, the 1× frequency is dominant, and all the other harmonics, 2×, 3×, and 4×, remain weak. Figure 12(b) shows that the frequency spectrum of the piston rotational motion at 200 rpm has 12 harmonic modes with amplitudes of the tilt angle from 0.01° to 0.19°. There are eight harmonic modes of the piston lateral motion with amplitudes of the lateral displacement from 0.01 mm to 0.22 mm, as shown in Fig. 9(a). Figure 12(c) shows that seven harmonic modes of the piston rotational motion appear in the frequency spectrum at 300 rpm, while the piston lateral motion consists of four modes (Fig. 10(a)) at 300 rpm. For all the speeds investigated, the secondary motion is strong at the 1× frequency for both the rotational and lateral motion of the piston in the secondary motion. The frequency response of the components of the piston motion show that the piston secondary motion is in the mode consisting of a combination of piston rotational motion and piston lateral motion. All the amplitudes of the piston rotational motion and piston lateral motion shown are highest at the first harmonic mode. Piston rotational motion is dominant in the piston secondary motion and exhibits a unique characteristic of a high amplitude of the fifth harmonic. The dominance of the piston rotational motion is due to the offset of the piston pin location from the center of gravity of the piston, which caused the piston to rotate along the piston pin axis. It can be observed that the 2×, 5×, and 7× harmonics are becoming stronger as the engine speed increases, as shown in Fig. 12(c) for 300 rpm. More importantly, the lateral motion has become less harmonic, with an increase in the baseline level, at 300 rpm and 500 rpm, as shown in Figs. 10(a) and 11. This indicates that the signal for the lateral motion has transformed from simple harmonic motion to a complex, irregular motion superposed with the strong 1×, 2×, 5×, and 7× harmonics. This is an indication of the transition from the harmonic and periodic motion observed at low speeds to a more chaotic secondary motion as the speed increases. The same phenomenon has been reported by Farahanchi and Shaw [20]. The results

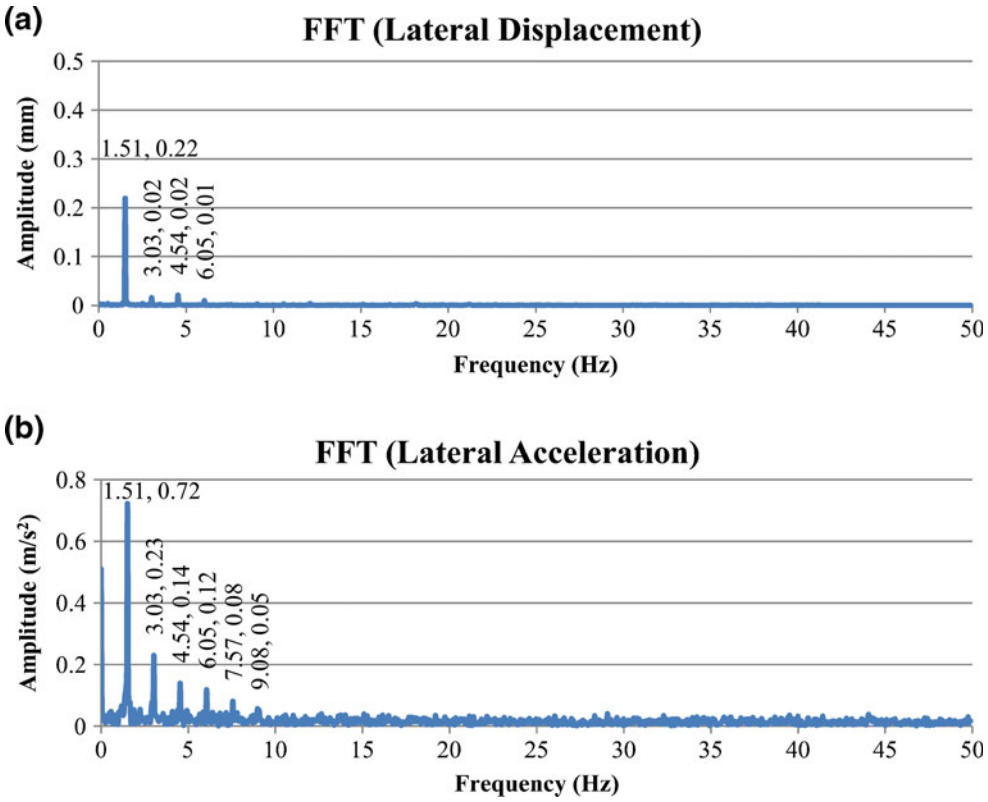

Fig. 8 Verification of lateral motion using lateral acceleration at 100 rpm

from their nonlinear model of secondary motion of the piston showed a distinct region of harmonic motion at low engine speeds, transitional motion at medium speeds, and chaotic motion at higher speeds. However, the results presented here can only be compared to their low and medium speed categories.

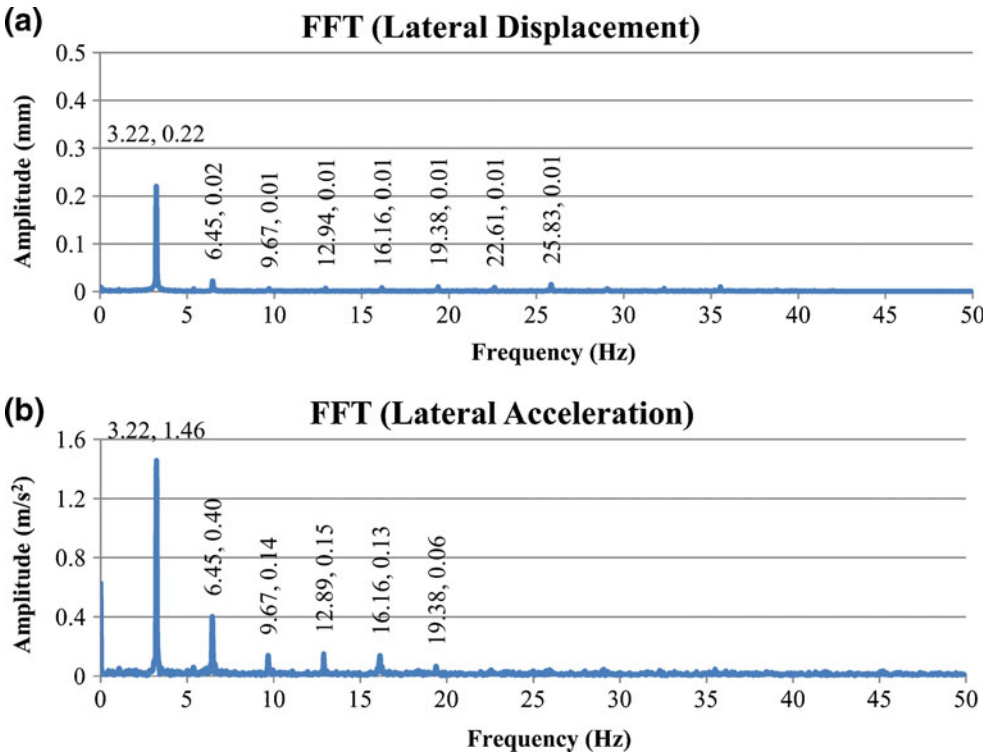

Fig. 9 Verification of lateral motion using lateral acceleration at 200 rpm

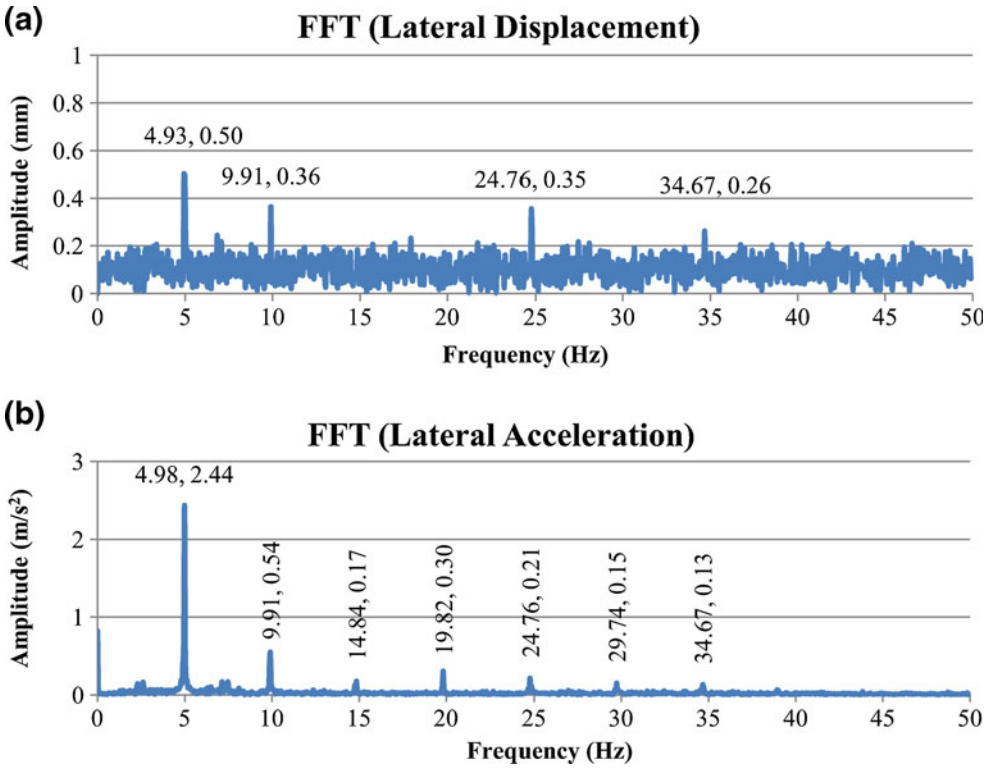

Fig. 10 Verification of lateral motion using lateral acceleration at 300 rpm

The exact influence of the piston ring on the secondary motion of the piston has not been studied before. Nakashima et al. [23] performed a study where a strain gauge was installed on both the top and second rings to measure the instantaneous increase in strain when the rings passed through the intake and exhaust ports. However, this study did not consider the piston secondary motion. In general, studies of the influence of the piston ring have been limited to the modeling of the contact stiffness and damping between the piston and the cylinder wall [9] and the friction effect between the piston and the cylinder wall [24–26]. However, the specific influence of the piston skirt is more dominant in the secondary motion of the piston than the influence of the piston ring [1]. The technique developed in this work can be used to determine the influence of the piston rings on the piston secondary motion, because it can be used to measure the piston motion with and without the piston ring pack or the motion of pistons with different locations of the top and second rings.

Conclusions

A laser displacement sensor has been developed to capture the distinct components of piston motion, such as the reciprocating, rotational, and lateral motions under non-firing conditions. The frequency component of the lateral displacement obtained from the laser displacement sensor was verified using the frequency component of the lateral acceleration measured by an accelerometer. The developed system was able to capture

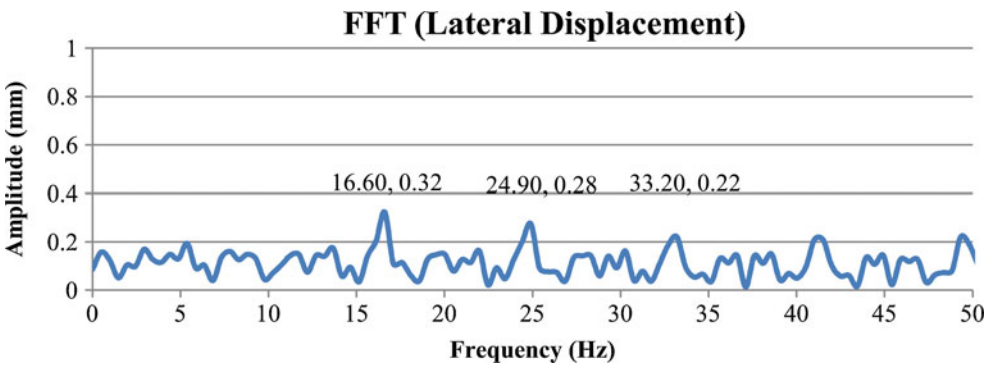

Fig. 11 FFT of piston lateral motion at 500 rpm

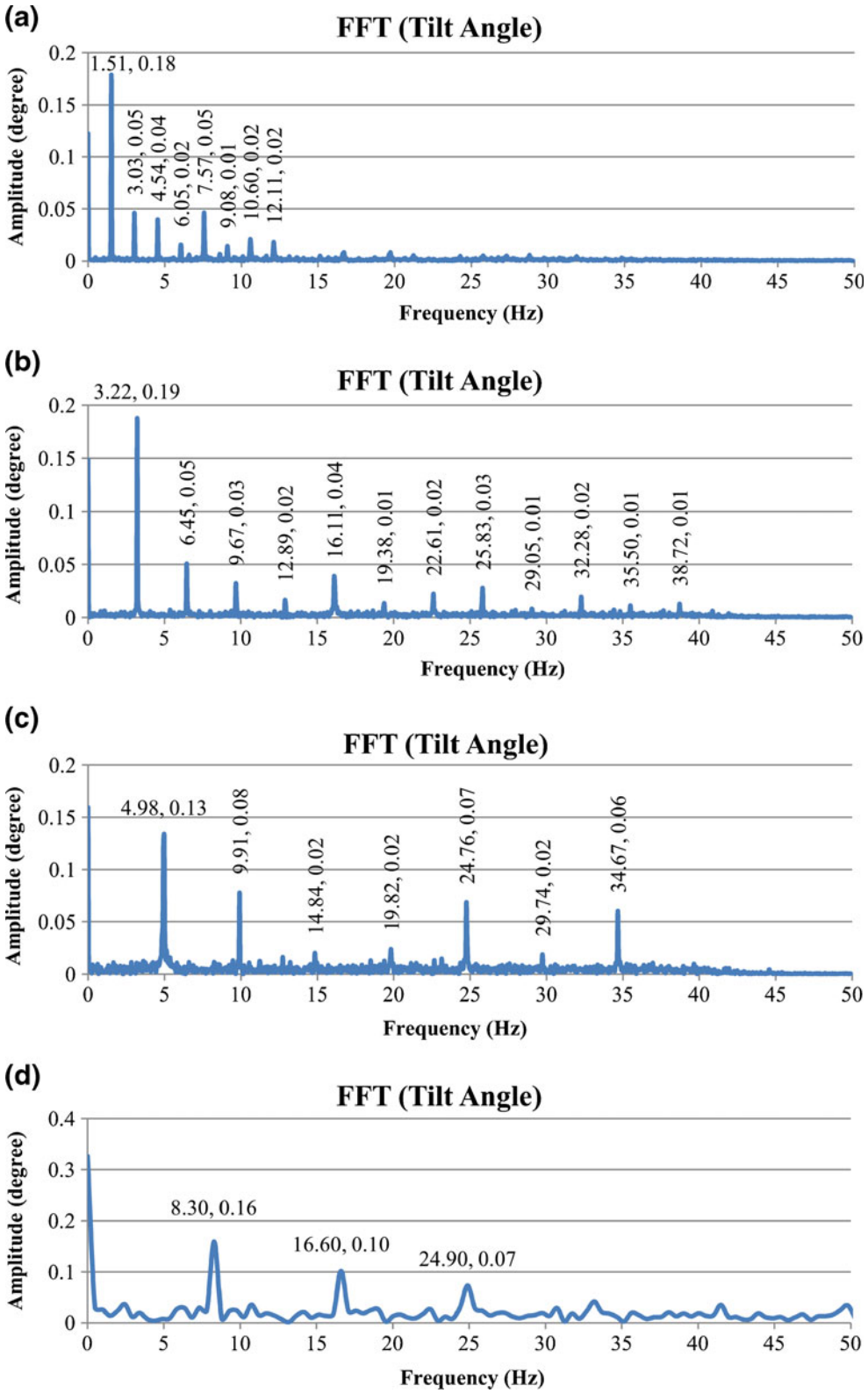

Fig. 12 FFT of piston rotational motion at **(a)** 100 rpm, **(b)** 200 rpm, **(c)** 300 rpm, and (d) 500 rpm

all the modes of the piston secondary motion. The results showed that the piston secondary motion consists of harmonics, where the first harmonics are strongest for both the rotational and lateral motion. Within the speed range below 500 rpm, the piston secondary motion is shown to be periodic.

Acknowledgments This research has been carried out with financial support from USM fellowship and USM-RU-PRGS grant A/C 1001/PMEKANIK/8034012.

References

1. Cho SH, Ahn ST, Kim YH (2002) A simple model to estimate the impact force induced by piston slap. J Sound Vib 255(2):229–242. doi:10.1006/jsvi.2001.4152
2. Flores P, Ambrósio J, Claro J, Lankarani H (2008) Translational joints with clearance in rigid multibody systems. J Comput Nonlinear Dyn 3:011007. doi:10.1115/1.2802113
3. Haddad SD, Tjan KT (1995) An analytical study of offset piston and crankshaft designs and the effect of oil film on piston slap excitation in a diesel engine. Mech Mach Theory 30(2):271–284. doi:10.1016/0094-114X(94)00035-J
4. Andersson P, Tamminen J, Sandström CE (2002) Piston ring tribology. A literature survey, VTT Research Notes 2178
5. Wilson R, Fawcett JN (1974) Dynamics of the slider-crank mechanism with clearance in the sliding bearing. Mech Mach Theory 9 (1):61–80. doi:10.1016/0094-114x(74)90008-1
6. Khemili I, Romdhane L (2008) Dynamic analysis of a flexible slider-crank mechanism with clearance. Eur J Mech Solid 27 (5):882–898. doi:10.1016/j.euromechsol.2007.12.004
7. Kim TJ (2003) Numerical analysis of the piston secondary dynamics in reciprocating compressors. J Mech Sci Technol 17(3):350–356. doi:10.1007/BF02984361
8. Cho JR, Moon SJ (2005) A numerical analysis of the interaction between the piston oil film and the component deformation in a reciprocating compressor. Tribol Int 38(5):459–468. doi:10.1016/j.triboint.2004.10.002
9. Geng Z, Chen J (2005) Investigation into piston-slap-induced vibration for engine condition simulation and monitoring. J Sound Vib 282(3–5):735–751. doi:10.1016/j.jsv.2004.03.057
10. Zhang Z, Xie Y, Zhang X, Meng X (2009) Analysis of piston secondary motion considering the variation in the system inertia. Proc Inst Mech Eng, Part D: J Automob Eng 223(4):549–563. doi:10.1243/09544070JAUTO1078
11. Zhang X, Zhang Z, Wang P, Xie Y (2008) A piston lubrication model considering the coupling between the piston secondary motion and the system inertia variation in an IC engine. Proceedings of CIST 2008 & ITS-IFToMM 2008 Beijing, China:191–196. doi:10.1007/978-3-642-03653-8_65
12. Zhou X, Cai G, Cheng Z, Zhang Z (2010) A coupling model for dynamic and tribological behaviors of piston system in IC engine. Proceedings of Intelligent Systems and Applications 2010, Wuhan, China:1–5. doi:10.1109/IWISA.2010.5473586
13. McFadden P, Turnbull S (2011) Dynamic analysis of piston secondary motion in an internal combustion engine under non-lubricated and fully flooded lubricated conditions. Proc Inst Mech Eng, Part C: J Mech Eng Sci. doi:10.1177/0954406211408674
14. Comfort A (2003) An introduction to heavy-duty diesel engine frictional losses and lubricant properties affecting fuel economy - Part I. SAE International 2003-01-3225
15. Taylor R, Coy R (2000) Improved fuel efficiency by lubricant design: a review. Proc Inst Mech Eng, Part J: J Eng Tribol 214 (1):1–15. doi:10.1177/135065010021400101
16. Wang Y, Yao C, Barber GC, Zhou B, Zou Q (2005) Scuffing resistance of coated piston skirts run against cylinder bores. Wear 259(7–12):1041–1047. doi:10.1016/j.wear.2004.12.005
17. Ye Z, Zhang C, Wang Y, Cheng HS, Tung S, Wang QJ, He X (2004) An experimental investigation of piston skirt scuffing: a piston scuffing apparatus, experiments, and scuffing mechanism analyses. Wear 257(1–2):8–31. doi:10.1016/s0043-1648(03)00538-6
18. Tan Y-C, Ripin ZM (2011) Frictional behavior of piston rings of small utility two-stroke engine under secondary motion of piston. Tribol Int 44(5):592–602. doi:10.1016/j.triboint.2010.12.009
19. Online FAMOS Function-reference (2006). imc Meßsysteme GmbH imcDevices version 2.6R1
20. Farahanchi F, Shaw SW (1994) Chaotic and periodic dynamics of a slider-crank mechanism with slider clearance. J Sound Vib 177 (3):307–324. doi:10.1006/jsvi.1994.1436
21. Rahnejat H, Balakrishnan S, King P, Howell-Smith S (2006) In-cylinder friction reduction using a surface finish optimization technique. Proc Inst Mech Eng, Part D: J Automob Eng 220 (9):1309–1318. doi:10.1243/09544070JAUTO282
22. Flores P, Leine R, Glocker C (2010) Modeling and analysis of planar rigid multibody systems with translational clearance joints based on the non-smooth dynamics approach. Multibody Syst Dyn 23(2):165–190. doi:10.1007/s11044-009-9178-y
23. Nakashima K, Nakano Y, Ishihara S, Murakami Y, Yamamoto M (2010) Behavior of piston rings passing over cylinder ports in two-stroke cycle engines. J Mech Sci Technol 24(1):227–230. doi:10.1007/s12206-009-1173-y
24. Guzzomi A, Hesterman D, Stone B (2007) The effect of piston friction on engine block dynamics. Proc Inst Mech Eng, Part K: J Multi-body Dyn 221(2):277–289. doi:10.1243/14644193JMBD66
25. Livanos GA, Kyrtatos NP (2007) Friction model of a marine diesel engine piston assembly. Tribol Int 40(10–12):1441–1453. doi:10.1016/j.triboint.2007.01.020
26. Zweiri Y, Whidborne J, Seneviratne L (2000) Instantaneous friction components model for transient engine operation. Proc Inst Mech Eng, Part D: J Automob Eng 214(7):809–824. doi:10.1243/0954407001527664